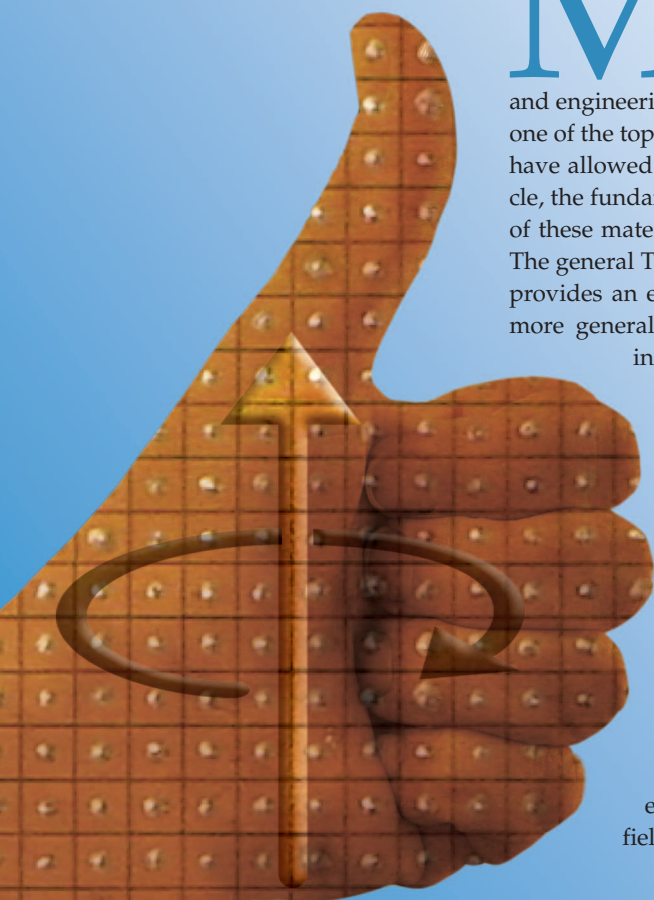# Composite Right/Left-Handed Transmission Line Metamaterials

©DIGITAL VISION

Metamaterials are artificial structures that can be designed to exhibit specific electromagnetic properties not commonly found in nature. Recently, metamaterials with simultaneously negative permittivity (ε) and permeability (μ), more commonly referred to as left-handed (LH) materials, have received substantial attention in the scientific and engineering communities. *Science* magazine even named LH materials (LHMs) as one of the top ten scientific breakthroughs of 2003 [1]. The unique properties of LHMs have allowed novel applications, concepts, and devices to be developed. In this article, the fundamental electromagnetic properties of LHMs and the physical realization of these materials are reviewed based on a general transmission line (TL) approach. The general TL approach provides insight into the physical phenomena of LHMs and provides an efficient design tool for LH applications. LHMs are considered to be a more general model of composite right/left hand (CRLH) structures, which also include right-handed (RH) effects that occur naturally in practical LHMs. Characterization, design, and implementation of one-dimensional (1-D) and two-dimensional (2-D) CRLH TLs are examined. In addition, novel microwave devices based on CRLH TLs and their applications are presented.

LHMs

The concept of LHMs was first theorized by the Russian physicist Veselago in 1967 [2] (Veselago's paper was translated into English in 1968; the translated paper mistakenly notes 1964 as the original year of publication). In his paper, Veselago speculated on the possible existence of LHMs and anticipated their unique electromagnetic properties such as the reversal of Snell's Law, the Doppler effect, and the Vavilov-Cerenkov effect (radiation produced by a fast-moving particle as it travels through a medium). Veselago showed that the electric field, magnetic field, and wavevector of an electromagnetic wave in an LHM form an LH

*Anthony Lai (antlai@ee.ucla.edu) and Tatsuo Itoh are with
the Electrical Engineering Department, University of California, Los Angeles, CA 90095 USA.
Christophe Caloz is with the Département de Génie Électrique,
École Polytechnique de Montréal, Montréal, Québec H3T 2B1, Canada.*

Anthony Lai, Christophe Caloz, and Tatsuo Itoh

triad. As a result, LHMs support electromagnetic waves with group and phase velocities that are antiparallel, known as backward waves [3]. Consequently, while energy still travels away from the source, so as to satisfy causality, wavefronts travel backward toward the source in an LHM, a phenomenon which is associated with negative index of refraction.

Although Veselago predicted the existence of LHMs, experimental verification of LHMs did not occur until three decades later by a group at University of California, San Diego (UCSD). The UCSD's LHM consisted of copper split-ring resonators (SRRs) and thin copper wires, providing negative permeability and negative permittivity, respectively [4]. By constructing a wedge-shaped structure with their SRR-based LHM, the group at USCD demonstrated the concept of a negative index of refraction. A group at Massachusetts Institute of Technology (MIT) repeated this experiment, confirming UCSD's findings [5]. Following these experimental verifications, several researchers have further studied the characteristics and applications of SRR-based LHMs [6]–[8]. However, since resonant structures such as SRRs are lossy and narrow-banded, they are often difficult to implement for microwave applications. Several researchers soon realized that a TL approach towards LHMs was possible [9], [10]. The TL approach of LHMs, presented in this article, has led to nonresonant structures with lower loss and wider bandwidth. In particular, metamaterials with RH and LH properties known as CRLH metamaterials have led to the development of several novel microwave devices which are discussed in this article.

CRLH Theory

TL theory has long been a powerful analysis and design tool for conventional (i.e., RH) materials. By modeling a CRLH metamaterial as an equivalent TL, TL theory can be used to analyze and design 1-, 2-, or even 3-D CRLH metamaterials. In the following sections, the TL approach to CRLH metamaterials will be developed. First, the CRLH metamaterial will be represented by an equivalent homogeneous (continuous and invariant along the direction of propagation) CRLH TL to gain immediate insight into its fundamental characteristics. Then, an LC network implementation of the TL will be developed, since homogeneous CRLH structures do not appear to exist in nature. The LC network provides a realistic description of the CRLH metamaterial. Finally, physical realizations of the LC network will be discussed. For simplicity, only the lossless TL will be examined.
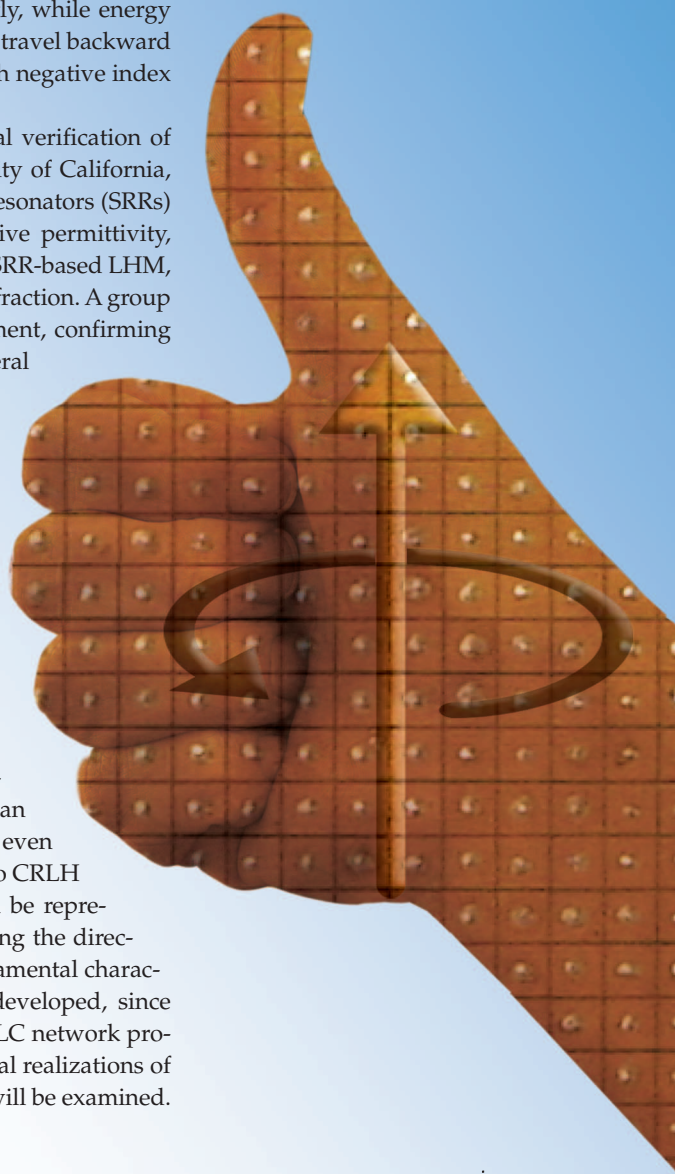
Homogeneous Case

The homogeneous models of a purely RH (PRH), purely LH (PLH), and CRLH lossless TL are shown in Figure 1(a), (b), and (c), respectively. The PRH TL model, shown in Figure 1(a), can be represented as the combination of a per-unit length series inductance L'_R and a per-unit length shunt capacitance C'_R. The PLH TL model, shown in Figure 1(b), is the combination of a times-unit length series capacitance C'_L and a times-unit length shunt inductance L'_L and is the dual of the PRH TL. In reality, a PLH structure is not possible because of unavoidable RH parasitic series inductance (L) and shunt capacitance (C) effects (parasitic capacitance is due to development of voltage gradients, and unavoidable parasitic inductance is due to current flow along the metallization). Therefore, a CRLH structure represents the most general form of a structure with LH attributes.
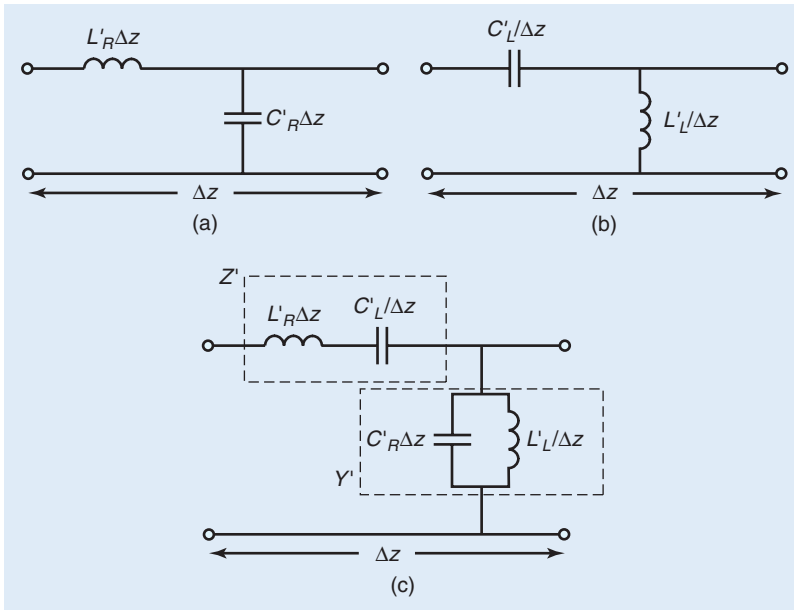

Figure 1. *Equivalent circuit model. (a) Homogeneous RH TL. (b) Homogeneous LH TL. (c) Homogeneous CRLH TL.*

The general CRLH TL model shown in Figure 1(c) consists of an inductance L'_R in series with a capacitance C'_L and a shunt capacitance C'_R in parallel with an inductance L'_L.

The propagation constant of a TL is given by $\gamma = \alpha + j\beta = \sqrt{Z'Y'}$, where Z' and Y' are, respectively, the per-unit length impedance and per-unit length admittance. In the particular case of the CRLH TL, Z' and Y' are defined as

$$Z'(\omega) = j\left(\omega L'_R - \frac{1}{\omega C'_L}\right),$$

$$Y'(\omega) = j\left(\omega C'_R - \frac{1}{\omega L'_L}\right). \quad (1)$$

Therefore, the dispersion relation for a homogenous CRLH TL is

$$\beta(\omega) = s(\omega)\sqrt{\omega^2 L'_R C'_R + \frac{1}{\omega^2 L'_L C'_L} - \left(\frac{L'_R}{L'_L} + \frac{C'_R}{C'_L}\right)}, \quad (2)$$

where

$$s(\omega) = \begin{cases} -1 & \text{if } \omega < \omega_{\Gamma 1} = \min\left(\frac{1}{\sqrt{L'_R C'_L}}, \frac{1}{\sqrt{L'_L C'_R}}\right) \\ +1 & \text{if } \omega > \omega_{\Gamma 2} = \max\left(\frac{1}{\sqrt{L'_R C'_L}}, \frac{1}{\sqrt{L'_L C'_R}}\right). \end{cases} \quad (3)$$

The phase constant β in (2) can be purely real or purely imaginary depending on whether the radicand is positive or negative, respectively. In the frequency range where β is purely real, a pass-band is present since $\gamma = j\beta$. In contrast, a stop-band occurs in the frequency range where β is purely imaginary since $\gamma = \alpha$.

This stop-band is a unique characteristic of the CRLH TL, which is not present in the PRH or the PLH cases.

Figure 2(a), (b), and (c) shows the $\omega - \beta$ or dispersion diagram of a PRH TL, PLH TL, and CRLH TL, respectively. The group velocity ($v_g = \partial\omega/\partial\beta$) and phase velocity ($v_p = \omega/\beta$) of these TLs can be inferred from the dispersion diagram. These diagrams show that v_g and v_p for a PRH TL are parallel ($v_g v_p > 0$), while v_g and v_p for a PLH TL are antiparallel ($v_g v_p < 0$). In addition, the CRLH TL's dispersion diagram shows that it has an LH ($v_g v_p < 0$) and RH ($v_g v_p > 0$) region. Figure 2(c) also illustrates the stop-band that occurs when γ is purely real for a CRLH TL.

In general, the series and shunt resonances of the CRLH TL are different. This is called the unbalanced case. However, when the series and shunt resonances are equal

$$L'_R C'_L = L'_L C'_R, \quad (4)$$

the LH and RH contribution exactly balance each other at a given frequency, as it will be shown shortly. Therefore, this condition is called the balanced case, and the resulting simplified circuit model is shown in Figure 3(a). It can be shown that under condition (4), the propagation constant in (2) reduces to the simpler expression

$$\beta = \beta_R + \beta_L = \omega\sqrt{L'_R C'_R} - \frac{1}{\omega\sqrt{L'_L C'_L}}, \quad (5)$$

where the phase constant distinctly splits up into the RH phase constant β_R and the LH phase constant β_L. The

CRLH TL is increasingly dispersive as frequency increases, since the phase velocity ($v_p = \omega/\beta$) becomes increasingly dependent on frequency, as shown in (5), which also illustrates the dual nature of the CRLH TL; at low frequencies the CRLH TL is dominantly LH, while at high frequencies the CRLH TL is dominantly RH. The balanced CRLH TL's dispersion diagram of Figure 3(b) indicates that an LH to RH transition occurs at

$$\omega_0 \overset{\text{unbalanced}}{=} \frac{1}{\sqrt[4]{L'_R C'_R L'_L C'_L}} \overset{\text{balanced}}{=} \frac{1}{\sqrt{L'C'}}, \qquad (6)$$

where ω_0 is referred to as the transition frequency. Thus, there is a seamless transition from LH to RH for the balanced case, because γ is always purely imaginary, unlike the unbalanced case. As a result, the balanced CRLH TL's dispersion curve does not have a stop-band. Although β is zero at ω_0, which corresponds to an infinite guided wavelength ($\lambda_g = 2\pi/|\beta|$), wave propagation still occurs since v_g is nonzero at ω_0. In addition, at ω_0 the phase shift for a TL of length d is zero ($\phi = -\beta d = 0$). Phase advance ($\phi > 0$) occurs in the LH frequency range ($\omega < \omega_0$), and phase delay ($\phi < 0$) occurs in the RH frequency range ($\omega > \omega_0$).

The characteristic impedance of a TL is given by $Z_o = \sqrt{Z'/Y'}$. For the CRLH TL, the characteristic impedance is

$$Z_o \overset{\text{unbalanced}}{=} Z_L \sqrt{\frac{L'_R C'_L \omega^2 - 1}{L'_L C'_R \omega^2 - 1}} \overset{\text{balanced}}{=} Z_L = Z_R, \qquad (7a)$$

$$Z_L = \sqrt{\frac{L'_L}{C'_L}}, \qquad (7b)$$

$$Z_R = \sqrt{\frac{L'_R}{C'_R}}, \qquad (7c)$$

where Z_L and Z_R are the PLH and PRH impedances, respectively. Whereas the characteristic impedance for the unbalanced case is frequency dependent, (7a) indicates that the balanced case is frequency independent and, therefore, can be matched over a wide bandwidth.

The TL relations derived above can be related to the constitutive parameters of a CRLH material. As stated above, the propagation constant of a TL is $\gamma = j\beta = \sqrt{Z'Y'}$. Since the propagation constant of a material is $\beta = \omega\sqrt{\mu\varepsilon}$, the following relation can be set up:

$$-\omega^2 \mu\varepsilon = Z'Y'. \qquad (8)$$

Similarly, the TL's characteristic impedance $Z_o = \sqrt{Z'/Y'}$ can be related to the material's intrinsic impedance $\eta = \sqrt{\mu/\varepsilon}$ by

$$Z_o = \eta \quad \text{or} \quad \frac{Z'}{Y'} = \frac{\mu}{\varepsilon}, \qquad (9)$$

which with (8) relates the permeability and permittivity of a material to the impedance and admittance of its equivalent TL model

$$\mu = \frac{Z'}{j\omega} = L'_R - \frac{1}{\omega^2 C'_L}, \qquad (10a)$$

$$\varepsilon = \frac{Y'}{j\omega} = C'_R - \frac{1}{\omega^2 L'_L}. \qquad (10b)$$

The index of refraction ($n = c\beta/\omega$) for the balanced and unbalanced CRLH TL is displayed in Figure 4. This figure shows that the CRLH TL has a negative index of refraction in its LH range and a positive index of refraction in its RH range.

LC Network
The homogeneous CRLH TL does not appear to exist in nature. However, CRLH TLs that are effectively
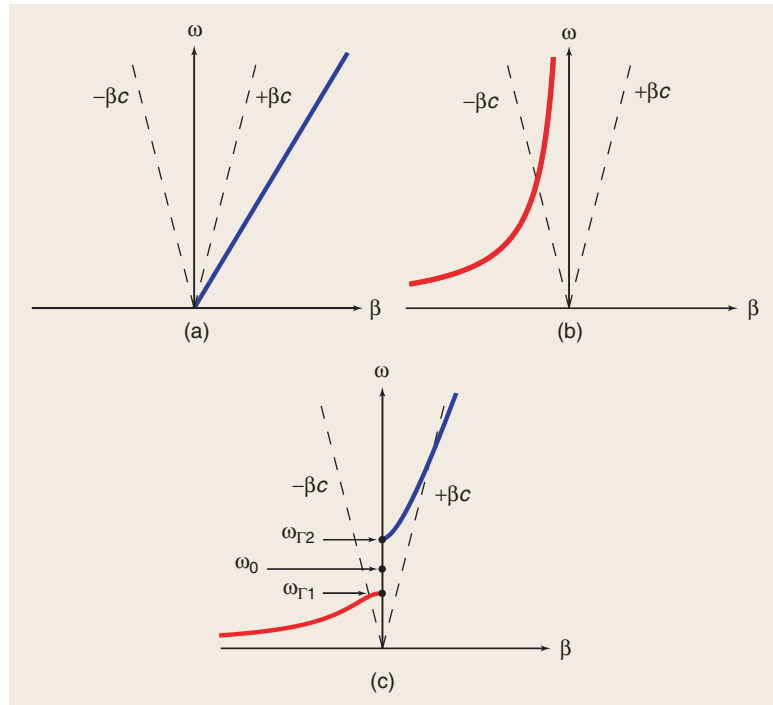

Figure 2. Dispersion diagrams for the TLs of Figure 1. (a) Homogeneous RH TL [11]. (b) Homogeneous LH TL [11]. (c) Homogeneous CRLH TL (unbalanced).
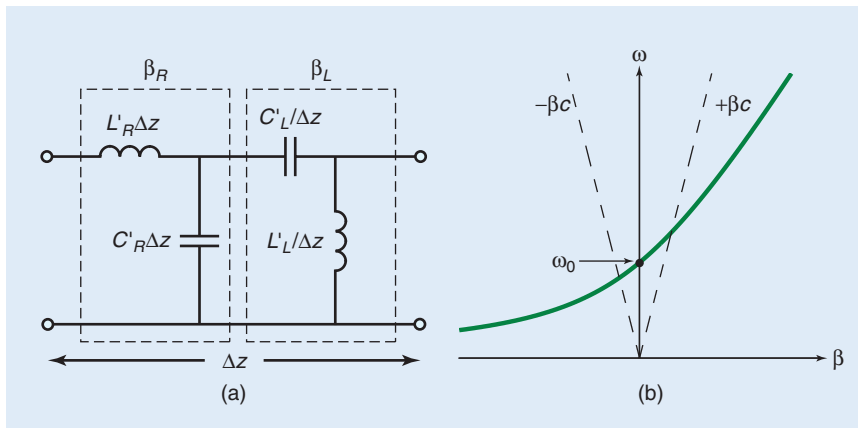
Figure 3. *Balanced form of Figure 1(c). (a) Simplified equivalent circuit model. (b) Dispersion diagram showing seamless LH to RH transition [11].*
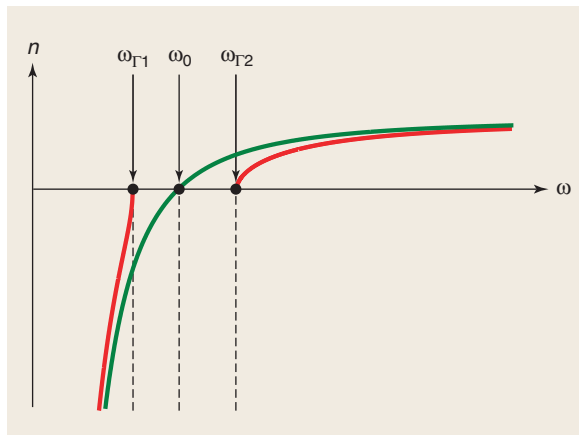

Figure 4. *Typical index of refraction plots for the balanced (green) and unbalanced (red) CRLH TL.*

homogenous—when an electromagnetic wave does not "see" discontinuities of the structure, because the guided wavelength is much larger than them—in a certain range of frequencies can be manufactured. An effectively homogeneous CRLH TL of length d can be constructed by cascading the band-pass LC unit cell of Figure 5(a) in either a nonperiodic or periodic fashion. Usually periodicity is preferred for computational and fabrication convenience of the CRLH TL [11].

The unit cell of Figure 5(a) is dimensionless, unlike the incremental model of Figure 1(c), which has an infinitesimal physical length of Δz (in meters). The phase of the LC unit cell can only be described in terms of its electrical length, $\theta = \Delta\phi$ (rad). However, a physical length p will be eventually associated with a practical implementation of the inductors and capacitors used [The LC unit cell's physical dimensions depend on the technology used (e.g., microstrip, coplanar waveguide, surface mount components, etc.)]. In the limit $p = \Delta z \to 0$, the LC unit cell of Figure 5(a) is equivalent to the incremental model of Figure 1(c). Therefore, a TL equivalent to an ideal homogeneous CRLH TL of length d can be formed by cascading the LC unit cell with the homogeneity condition $p \to 0$, as shown in Figure 5(b) [11]. The homogeneity condition
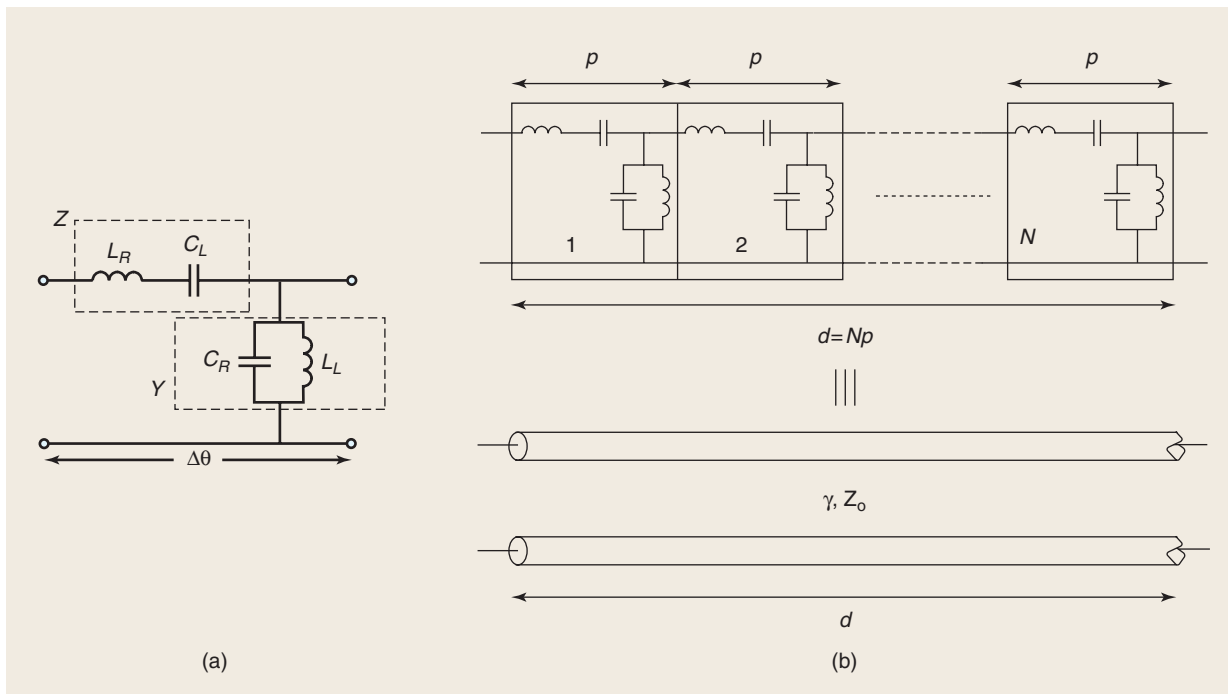

Figure 5. *LC-based CRLH TL. (a) Unit cell. (b) LC periodic network equivalent to a homogeneous CRLH TL of length d for $p = \Delta z \to 0$ [11].*

ensures that the TL appears homogeneous to the electromagnetic wave. In practice, if the unit cell is smaller than the guided wavelength $p < \lambda_g/4$, then the electrical length of the unit cell is smaller than $\pi/2$ and the LC-based CRLH TL is seen as effectively homogeneous by electromagnetic waves [11].

By applying periodic boundary conditions (PBCs) related to the Bloch-Floquet theorem to the LC unit cell [11], the LC dispersion relation

$$\beta(\omega) = \frac{1}{p} \cos^{-1}\left(1 + \frac{ZY}{2}\right) \qquad (11)$$

is obtained, where the series impedance (Z) and shunt admittance (Y) of the LC unit cell are given by

$$Z(\omega) = j\left(\omega L_R - \frac{1}{\omega C_L}\right), \quad Y(\omega) = j\left(\omega C_R - \frac{1}{\omega L_L}\right). \qquad (12)$$

Since the electrical length of the unit cell is small, the Taylor approximation $\cos(\beta p) \approx 1 - (\beta p)^2/2$ can be applied and (11) becomes

$$\beta(\omega) = \frac{s(\omega)}{p}\sqrt{\omega^2 L_R C_R + \frac{1}{\omega^2 L_L C_L} - \left(\frac{L_R}{L_L} + \frac{C_R}{C_L}\right)}, \qquad (13)$$

which is identical to the homogeneous dispersion relation of (2) (with $L'_R = L_R/p$, $C'_R = C_R/p$, $L'_L = L_L p$, $C'_L = C_L p$). This result shows that the LC-based

CRLH TL is equivalent to the homogeneous CRLH TL for small electrical lengths. The dispersion diagram for a balanced and unbalanced LC-based CRLH TL is shown in Figure 6. The LH portion of the dispersion curve was folded around the ω-axis to generate Figure 6.

This diagram shows that the band-pass LC-based CRLH TL exhibits a LH high-pass stop-band and a RH low-pass stop-band, unlike the ideal homogeneous CRLH TL, which does not exhibit any filter behavior. Although the LC-based CRLH TL is essentially a band-pass filter, the design of CRLH metamaterials has little to do with filter design for several reasons [11]. First, CRLH structures are designed to meet specific phase responses while filters are generally designed to meet magnitude
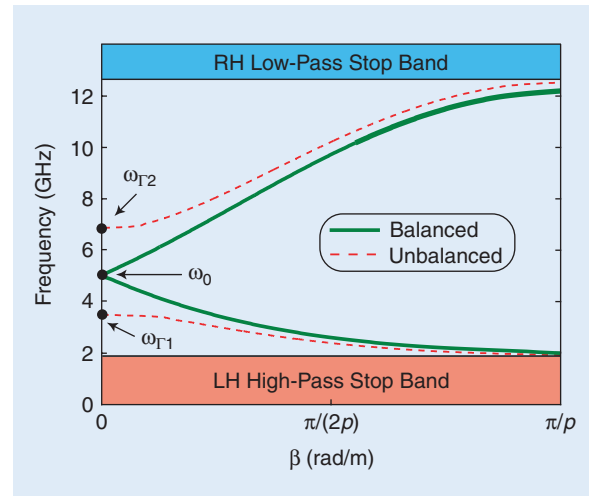

Figure 6. *Dispersion diagram for the balanced and unbalanced LC-based CRLH TL. Balanced: $L_R = L_L = 1$ nH, $C_R = C_L = 1$ pF; unbalanced: $C_R = 1$ pF, $C_L = 2$ pF [21].*
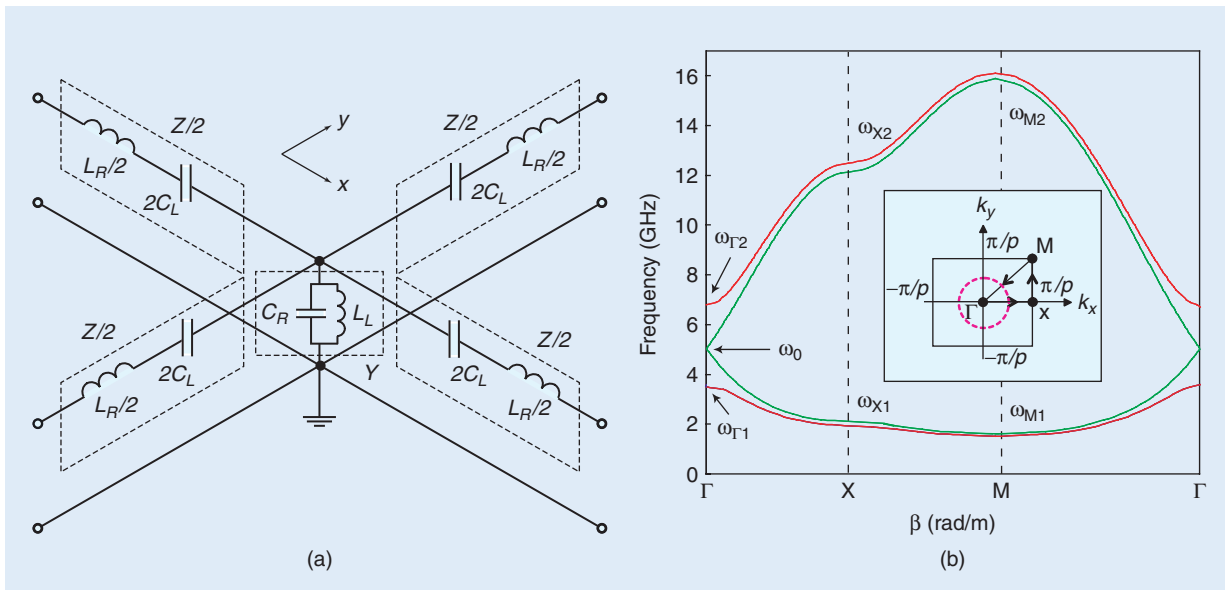

(a)   (b)

Figure 7. *2D CRLH TL. (a) Unit cell [11]. (b) Dispersion diagram for a balanced (green) and unbalanced (red) 2-D CRLH TL. Balanced: $L_R = L_L = 1$ nH, $C_R = C_L = 1$ pF; unbalanced: $L_R = 1$ nH, $L_L = 0.5$ nH, $C_R = 1$ pF, $C_L = 2$ pF. The inset shows the Brillouin zone of the 2-D periodic structure.*
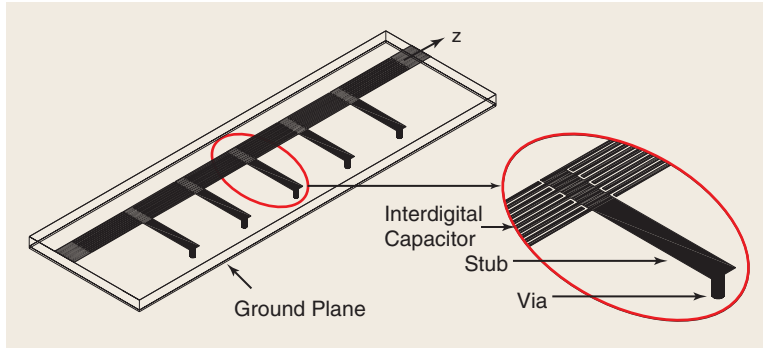
Figure 8. *A 1-D microstrip CRLH TL consisting of interdigital capacitors and shorted stub inductors [11].*

specifications. Secondly, as stated previously, the unit cell of CRLH metamaterials has to satisfy the homogeneity condition, $|\Delta\phi| < \pi/2$, but conventional filters usually do not need to satisfy this condition. In addition, conventional filters are 1-D, while CRLH metamaterials can be 2- or 3-D and behave as bulk media.

The 1-D CRLH TL can be extended to a 2-D CRLH TL [11], [12] by using the modified unit cell of Figure 7(a). Similar to the design of a 1-D CRLH TL, a 2-D CRLH TL can be constructed by repeating the 2-D unit cell of Figure 7(a) along two directions. The 2-D CRLH TL supports wave propagation in any direction within the structure. As a result, the phase constant β is a vector quantity for the 2-D CRLH TL, $\overrightarrow{\beta} = \hat{x}k_x + \hat{y}k_y$ where k_x and k_y are the propagation constants for the x and y directions. By applying PBCs to the 2-D unit cell along the x and y directions, the 2-D dispersion relation

$$\frac{(e^{-jk_x p} - 1)^2}{e^{-jk_x p}} + \frac{(e^{-jk_y p} - 1)^2}{e^{-jk_y p}} - ZY = 0, \quad (14)$$

is obtained, where the series impedance Z and shunt admittance Y of the unit cell are given by (12). This dispersion relation reduces to the 1-D dispersion relation of (11) when either k_x or k_y is zero.

Figure 7(b) shows the corresponding dispersion diagram and Brillouin zone [13] for the 2-D CRLH TL, where $\Gamma(k_x p = k_y p = 0)$, $X(k_x p = \pi, k_y p = 0)$, and $M(k_x p = k_y p = \pi)$ represent the high-symmetry points of the Brillouin zone. The structure is LH from $\omega_{\Gamma 1}$ to ω_{M1} and RH from $\omega_{\Gamma 2}$ to ω_{M2}, as seen in Figure 7(b). For the unbalanced case, a stop-band occurs between $\omega_{\Gamma 1}$ and $\omega_{\Gamma 2}$. The stop-band disappears for the balanced case and $\omega_{\Gamma 1} = \omega_{\Gamma 2} = \omega_0$.

Physical Implementation

The previous section presented the LC approach to create a 1- or 2-D CRLH TL. However, the LC network must be realized with physical components that can generate the required capacitances (C_R and C_L) and inductances (L_R and L_L). Currently, surface-mount technology (SMT) chip components or distributed components have been used to realize the LC network. Distributed components can be implemented via microstrip, stripline, coplanar waveguide, or another technology.

The choice of SMT chip or distributed components depends on several factors. In terms of analysis and design, SMT-based CRLH structures are generally easier and quicker to implement. SMT chip components are readily available and do not need to be designed and fabricated, unlike their distributed counterparts. However, SMT components are only available in dis-
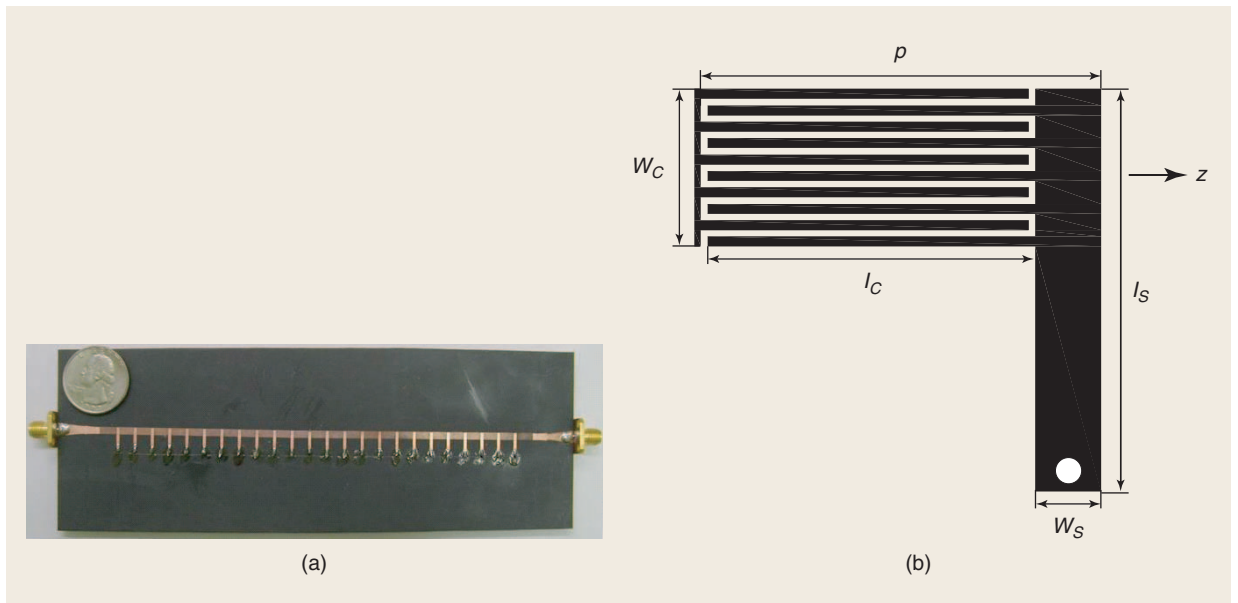

(a)

(b)

Figure 9. *24 unit-cell microstrip CRLH TL based on Figure 8. (a) Photograph of prototype. (b) Unit cell used for parameter extraction [11].*

crete values and are limited to low frequencies (3–6 GHz, depending on their values). As a result, specific phase responses and operational frequency ranges are limited for SMT-based CRLH structures. In addition, the choice between SMT chip and distributed components depends on the intended application. For example, SMT chip components are difficult to implement for radiation-type applications.

An example of a distributed component based 1-D CRLH TL is shown in Figure 8. This structure is implemented on microstrip with interdigital capacitors and stub inductors connected to the ground plane. The unit cell of the structure shown in the inset is equivalent to the circuit model of Figure 5(a). The interdigital capacitors and stub inductors provide the LH and also the RH contributions. In particular, the RH capacitance C_R is attributed to the capacitance between the trace and ground plane, and the RH inductance L_R is caused by the magnetic flux generated by the current flow in the digits of the interdigital capacitor.

A balanced, 24 unit-cell microstrip CRLH TL based on Figure 8 is displayed in Figure 9(a). The entire circuit was implemented on Rogers RT/Duroid 5880 with dielectric constant $\varepsilon_r = 2.2$ and thickness $h = 1.57$ mm. Parameter extraction was based on the unit cell of Figure 9(b) with $p = 6.1$ mm, $l_c = 5.0$ mm, $w_c = 2.4$ mm, $l_s = 8.0$ mm, $w_s = 1.0$ mm, and five pairs of digits with widths of 0.15 and 0.1 mm spacing. The extracted LH and RH parameters were $L_L = 3.38$ nH, $C_L = 0.68$ pF, $L_R = 2.45$ nH, and $C_R = 0.50$ pF. The experimental dispersion diagram is compared with the homogeneous TL relation (2) and LC network relation (11) in Figure 10.

One possible way of creating 2-D CRLH TL structures is by periodic repetition of the capacitively enhanced *mushroom* structure of Figure 11(a) [14]. The mushroom structure was first proposed by Sievenpiper

et al. [15] for the realization of high-impedance surfaces. Our group at UCLA demonstrated that Sievenpiper's mushroom structure is, in essence, a CRLH structure, capable of exhibiting a negative index of refraction [14]. The mushroom structure of Figure 11(a) is equivalent to the 2-D circuit model of Figure 7(a). The LH capacitance C_L is provided by the capacitance couplings of the top patch with adjacent patches, and the LH inductance is provided by a via connected to the ground plane. The caps are used to enhance the weak capacitance couplings between adjacent patches. The magnetic flux caused by the flow of current on the top patch contributes to the RH inductance L_R, while the parallel-plate structure between the patch and the ground plane contributes to the RH capacitance C_R. The 2-D CRLH structure of Figure 11(b) is open to air and can be implemented with microstrip.
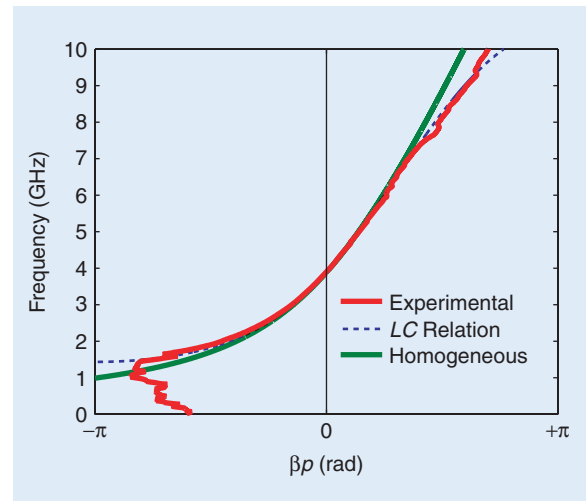

Figure 10. *Experimental dispersion diagram compared with the homogeneous TL relation (2) and LC network relation (11) for the 24-cell CRLH TL of Figure 9(a) [11].*
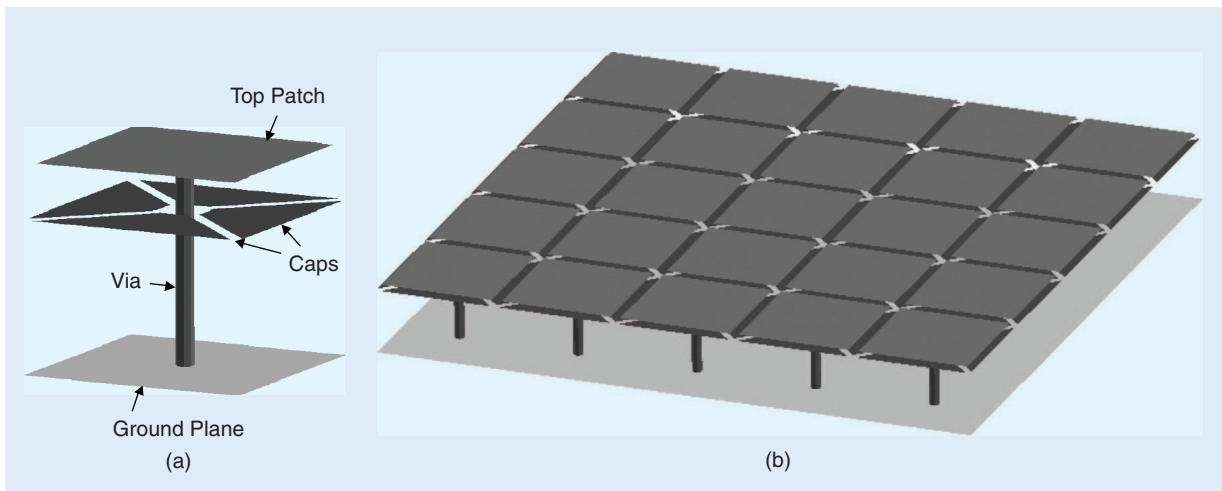

Figure 11. *Open 2-D CRLH mushroom structure. (a) Unit cell [14]. (b) 2-D CRLH structure formed by periodic repetition of the unit cell. The caps are floating (not connected to the vias) patches located at a short distance from the connected patch to enhance C_L contribution [14].*

The dispersion diagram of the open mushroom structure, shown in Figure 12, was generated by full-wave (FEM) simulation with unit cell parameters indicated in Figure 13. This dispersion diagram shows that the fundamental mode of the structure is a mixed LH–RH
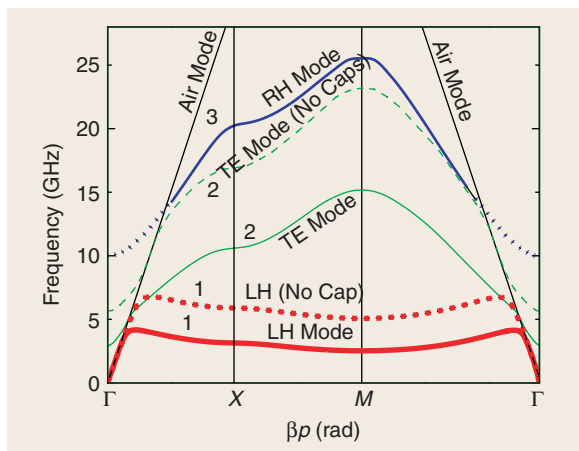

Figure 12. *Dispersion diagram (first 2–3 modes) of the CRLH mushroom unit cell of Figure 13 obtained by full-wave simulation (FEM) with PBCs. Dashed lines are for the open structure without the caps [14].*
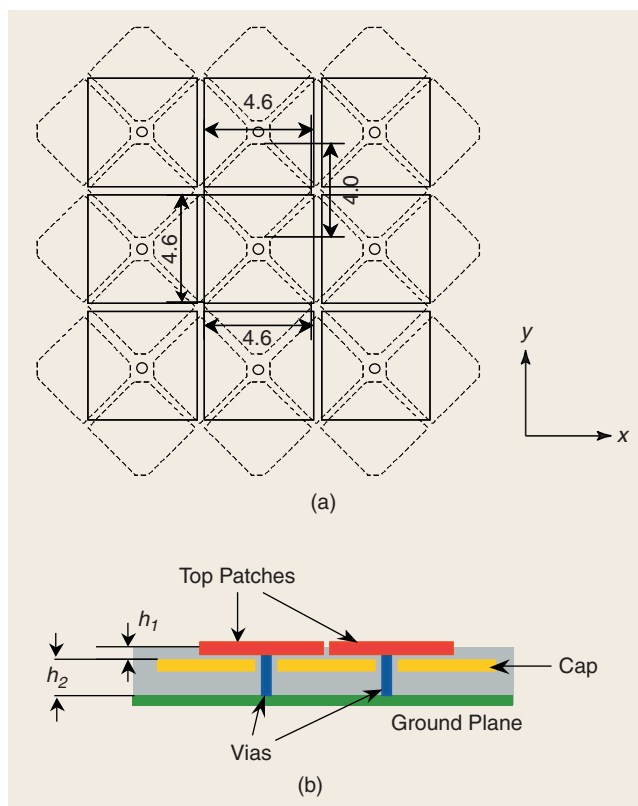

Figure 13. *Parameters of the mushroom structure to be analyzed. The period of the unit cell is 5.0 × 5.0 mm (square lattice $p_x = p_y = p$). The two substrates used have a relative permittivity of 2.2 and thicknesses of $h_1 = 0.127$ mm and $h_2 = 1.57$ mm, respectively. The diameter of the vias is 0.2 mm (their length is $h_1 + h_2 = 1.697$ mm). (a) Dimensions of the patches and caps [14]. (b) Cross-sectional view of the open structure [14].*

mode, because the LH mode of the open structure always couples with the TM air mode [16]. In contrast, a 2-D CRLH mushroom structure closed to air, which can be implemented by stripline, has a dominant mode that is purely LH [14]. The dispersion diagram also shows that the structure has two RH modes. However, the first RH mode is actually a degenerate TE mode and does not correspond to the RH mode of the circuit model, unlike the second RH mode. Figure 12 also shows that the LH mode is shifted towards higher frequencies when the caps are removed from the mushroom structure. The removal of the caps decreases the LH C_L contribution.

Microwave Applications

The CRLH TL has lead to several novel microwave applications and devices. This section presents guided, radiated, and refracted applications that utilize the unique features of CRLH TLs.

Guided Wave Applications

Dual-Band Branch-Line Coupler
Conventional branch-line couplers (BLCs) can only operate at their design frequency (f_1) and at their odd harmonics ($3f_1$). Since, dual-band wireless communication systems have operational frequencies separated by various/nonharmonic frequencies, the conventional BLC is not a practical solution for these systems. To overcome this drawback, the conventional BLC can be modified by replacing its RH TLs with CRLH TLs to yield a novel BLC with an arbitrary second operating frequency [17]. The advantage of the CRLH TL over the RH TL for a dual-band BLC can be seen in the phase-response diagram of Figure 14. Since the phase-response curve of the RH TL is a straight line from dc to f_1, the design frequency f_1 at $-90°$ determines the next usable frequency $3f_1$ at $-270°$. By changing the phase slope of the RH TL, the frequency at $-270°$ can be varied, but $-90°$ is no longer at the design frequency. Since the CRLH TL has a dc offset, it has an additional degree of freedom compared to the RH TL. By changing the dc offset and phase slope, the CRLH TL's phase-response curve can intercept a desired pair of phases at any arbitrary pair of frequencies (f_1, f_2) for dual-band operation.

Figure 15(a) shows a CRLH-based BLC with operational frequencies at $f_1 = 930$ MHz and $f_2 = 1,780$ MHz and corresponding phase delays of 90 and 270°, respectively. The CRLH TLs were implemented with SMT chip components. The magnitude response of the CRLH-based BLC is also shown in Figure 15(b); $|S_{21}|$ and $|S_{31}|$ of -3 dB are achieved at both operational frequencies.

In general, this CRLH dual-band concept can be applied to any microwave component (phase shifters, matching networks, baluns, etc.) [18].

Asymmetric Backward-Wave Directional Coupler

Conventional microstrip directional couplers are typically capable of operating over a broad bandwidth (>25%) but have loose coupling levels of −10 dB or less. Noncoupled-line couplers, such as branch-line and ring couplers, offer tight coupling levels (−3 dB) but at the expense of a lower bandwidth (<10%). The Lange coupler is able to achieve both broad bandwidth and tight coupling. However, it requires the use of cumbersome, expensive wire bonds. The novel coupler of Figure 16 offers an alternative to these conventional couplers [19]. It is capable of achieving any arbitrary coupling level over a 50% bandwidth without any wire bonds.

The novel coupler of Figure 16 is a quasi-0dB asymmetric coupler consisting of a CRLH line and a conventional microstrip ($C\mu S$) line implemented on Rogers RT/Duroid 5880 with dielectric constant $\varepsilon_r = 2.2$ and thickness $h = 1.57$ mm. This $C\mu S$/CRLH coupler consists of 9 CRLH unit cells of the type used in the CRLH TL of Figure 9(a). The spacing between the coupled lines is $s = 0.3$ mm, and the length of the coupler is $d = 62$ mm. By operating the CRLH line in its LH region, backward coupling is achieved. With reference to Figure 16, when an input signal is applied to Port 1, power (Poynting vector, S) propagates toward Port 2, but phase (propagation constant, β) travels toward Port 1. Since coupling to the conventional microstrip line results from evanescent waves in the transverse direction, the coupled power travels toward Port 3.

The $C\mu S$/CRLH coupler, like any conventional asymmetric coupler, is based on the phase differences between the c and π modes [20]. The coherence length (the length required for maximum coupling) of a conventional asymmetric coupler is given by

$$d_{\max} = \frac{\pi}{|\beta_c - \beta_\pi|}, \qquad (15)$$

where β_c and β_π are the c and π mode propagation constants. Under the assumption of weak coupling for the $C\mu S$/CRLH coupler, β_c is equal to the propagation constant of the CRLH TL ($\beta_c = \beta_{CRLH}$), and β_π is equal to the propagation constant of the conventional TL ($\beta_\pi = \beta_{C\mu S}$). Since β_{CRLH} is negative (LH region), the coherence length of the $C\mu S$/CRLH coupler is given by

$$d_{\max} = \frac{\pi}{|\beta_{CRLH}| + \beta_{C\mu S}}. \qquad (16)$$

Therefore, the $C\mu S$/CRLH coupler can achieve a much smaller coherence length than the conventional asymmetric coupler because of the plus sign in the
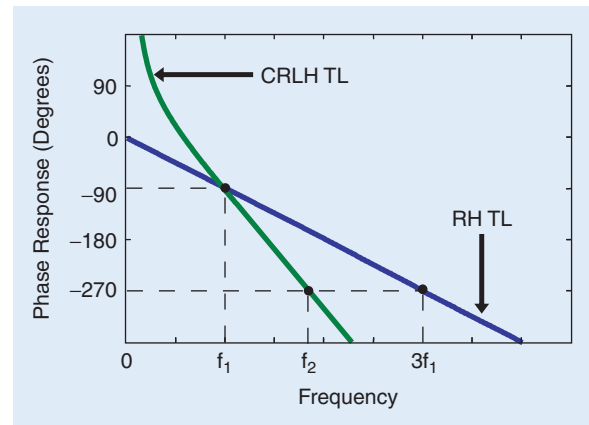

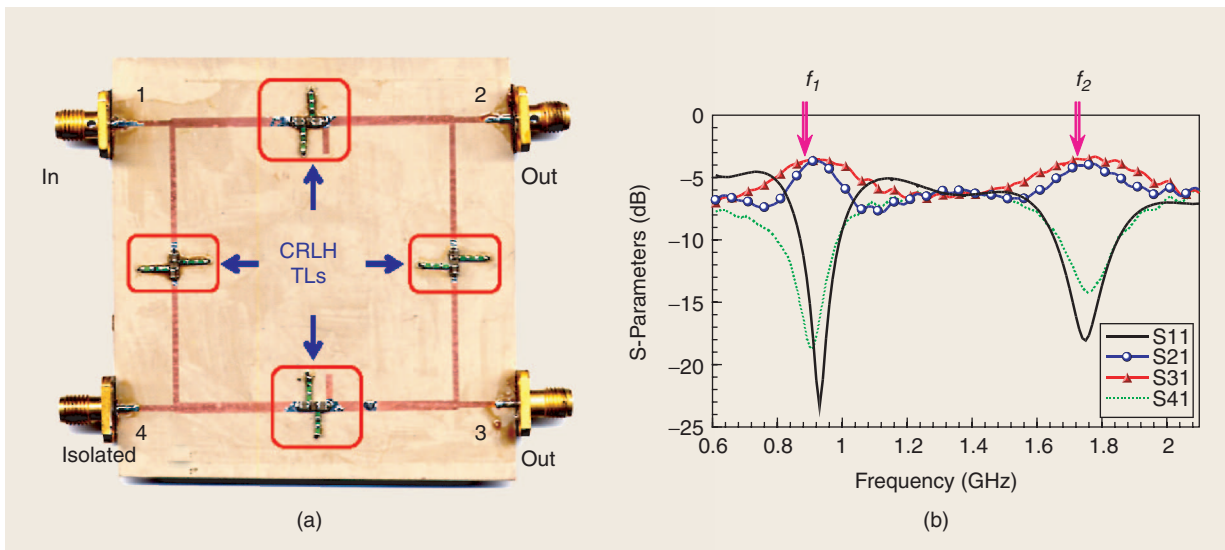**Figure 14.** *General phase response of a RH TL and a CRLH TL [17].*

Figure 15. *Dual-band BLC. (a) Photograph of completed dual-band BLC with CRLH TLs indicated [17]. (b) Measured S-parameters [17].*

denominator, which strongly reduces d_{max} in comparison to (15).

Figure 17 shows the performance of the $C\mu S$/CRLH coupler described above. Backward coupling of -0.7 dB is achieved over 2.2 GHz to 3.8 GHz, which represents a 53% bandwidth. A conventional coupler with an identical line spacing ($s = 0.3$ mm) can only provide a -10 dB coupling. By varying the number of CRLH unit cells or the line spacing, the $C\mu S$/CRLH coupler can achieve an arbitrary level of coupling. In [21], a symmetric CRLH coupler, based on a different principle than the coupler
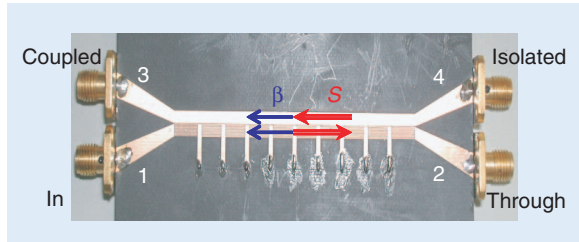

Figure 16. *Photograph of the nine-cell quasi-0dB asymmetric $C\mu S$/CRLH coupler. β and S represent the propagation and Poynting vector respectively in each line [19].*
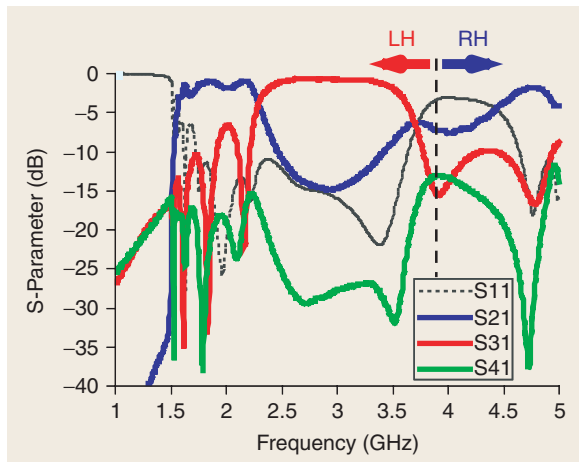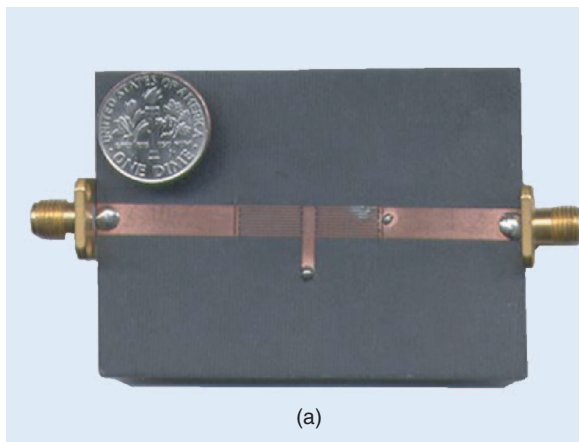

Figure 17. *Measured S-parameters of the quasi-0dB $C\mu S$/CRLH coupler. The CRLH transition frequency is $f_0 = 3.9$ GHz [19].*

of Figure 16, but achieving comparable performance was also demonstrated.

Zeroth Order Resonator

As mentioned above, a unique feature of CRLH metamaterials is that a β of zero can be achieved at a non-zero frequency. This property can be used to create a novel zeroth order resonator (ZOR) which is depicted in Figure 18(a) [22]. The resonator consists of one unit cell of Figure 8 open-ended by capacitive slits with parameters shown in Figure 18(b). The resonator was implemented on Rogers RT/Duroid 5880 substrate with dielectric constant $\varepsilon_r = 2.2$ and thickness $h = 1.57$ mm. At $\beta = 0$ there is no phase shift across the resonator since phase shift is determined by $\phi = -\beta d = 0$. In addition, it can be shown that the resonance is independent of the length of the structure but depends only on the reactive loadings.

The unloaded quality factor Q_0 of the ZOR depicted in Figure 18(a) is given by [22]

$$Q_o = \frac{\sqrt{C_R/L_L}}{G}, \tag{17}$$

where G is the shunt conductance of a lossy CRLH TL. Note that this quality factor is independent of the number of unit cells.

The measured resonance characteristic of the ZOR is compared with Method of Moments (MoM) simulation results in Figure 19. An unloaded quality factor $Q_0 = 250$ was obtained at 1.9 GHz, which is comparable to the unloaded quality factor of a conventional half-wavelength resonator on the same substrate and with the same resonant frequency [22].

Other Guided Wave Applications

Besides the above-mentioned applications, CRLH metamaterials can be applied to a variety of other guided-wave applications. Size reduction and bandwidth enhancement of conventional microwave components
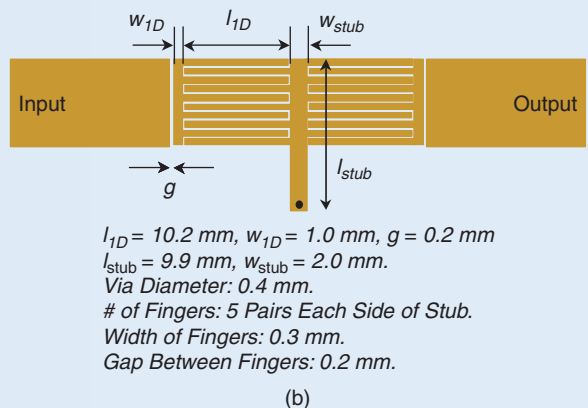

$l_{1D} = 10.2$ mm, $w_{1D} = 1.0$ mm, $g = 0.2$ mm
$l_{stub} = 9.9$ mm, $w_{stub} = 2.0$ mm.
Via Diameter: 0.4 mm.
# of Fingers: 5 Pairs Each Side of Stub.
Width of Fingers: 0.3 mm.
Gap Between Fingers: 0.2 mm.

(a)   (b)

Figure 18. *One-cell ZOR. (a) Photograph of prototype [22]. (b) Layout with parameters shown [22].*

can be achieved with the use of CRLH metamaterials. For example, by replacing the $270°$ branch of the conventional hybrid ring with a $-90°$ CRLH TL branch, the novel hybrid ring of [23] achieved a 50% bandwidth enhancement and a 67% size reduction over a conventional hybrid ring. In [24], the properties of nonlinear CRLH TLs, which are formed by incorporating nonlinear active devices (varactor diodes) to the CRLH TL, were investigated. The unique voltage response of the nonlinear CRLH TL can be potentially used to generate ultra-short pulses for ultra-wideband (UWB) systems. Finally, the guided-wave applications discussed so far utilized the passband region of the CRLH TL, in which permittivity and permeability are simultaneously positive or negative. However, the CRLH has either a negative permittivity $(-\varepsilon)$ or negative permeability $(-\mu)$ in its stop-band. By combining a $-\varepsilon$ CRLH TL with a $-\mu$ CRLH TL, a resonator independent of physical length similar to the ZOR was demonstrated in [25].

Radiated Wave Applications

Zeroth Order Resonator Antenna
The ZOR discussed above can be used to construct a ZOR antenna as shown in Figure 20 [26]. The microstrip-based unit cell consists of an interdigital capacitor and a shunt meander line connected to a rectangular patch. The rectangular patch behaves as a virtual ground plane.

Since resonance is independent of physical dimensions for the ZOR, the size of the antenna can be smaller than a half-wavelength. Instead, the antenna's size is determined by the reactive loadings in its unit cells. Figure 21 shows the size reduction that is possible with a ZOR antenna with a design frequency of 4.88 GHz. The size of the antenna is 10 mm, while the length of the $\lambda/2$

microstrip patch antenna with the same substrate and design frequency is 20.6 mm. The antenna of Figure 21(a) was implemented on a substrate with dielectric constant $\varepsilon_r = 2.68$ and thickness $h = 0.79$ mm. The period of the unit cell is 2.5 mm with four pairs of digits for the interdigital capacitors and three turns for the meander
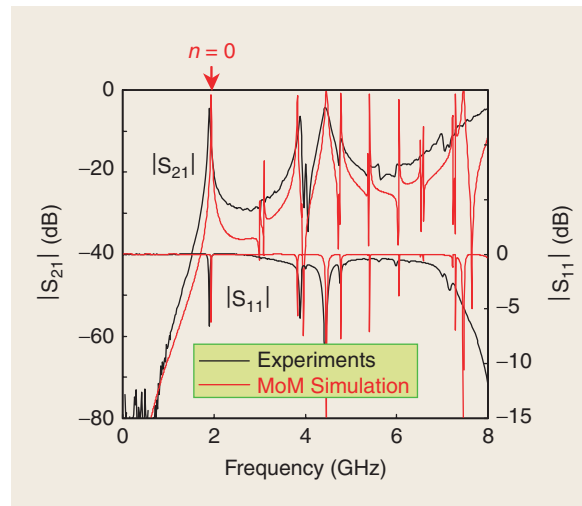

Figure 19. Measured and simulated $|S_{11}|$ and $|S_{21}|$ for the ZOR of Figure 18(a) [22].
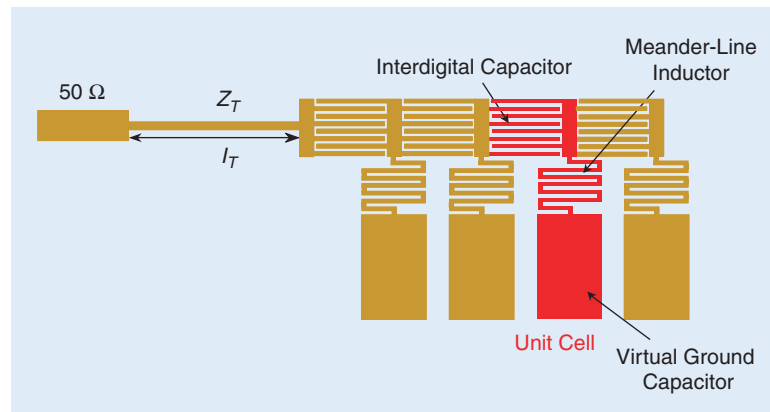

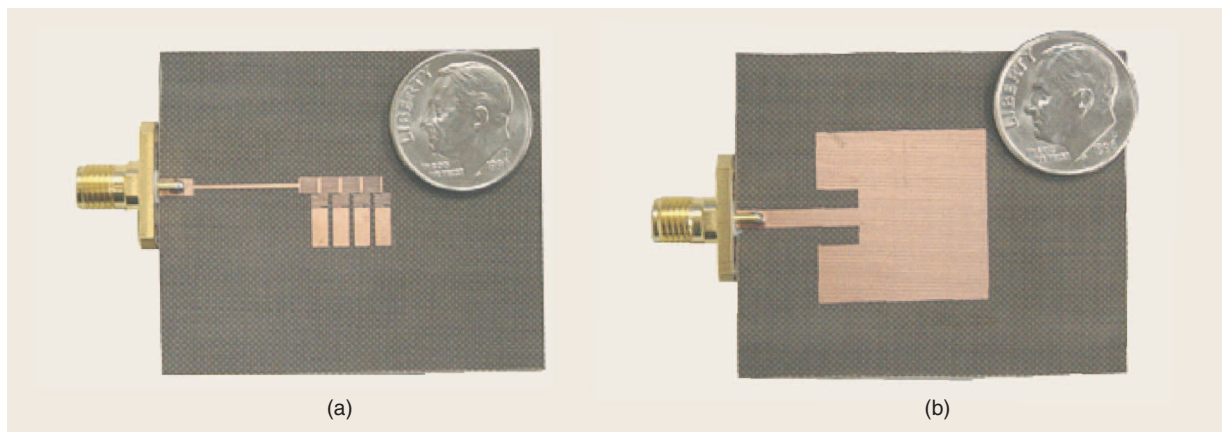**Figure 20.** Four-cell ZOR antenna layout [26].

Figure 21. Antenna comparison. (a) Four-cell ZOR antenna ($f_0 = 4.88$ GHz) [26]. (b) Microstrip patch antenna on the same substrate ($f_0 = 4.90$ GHz) [26].
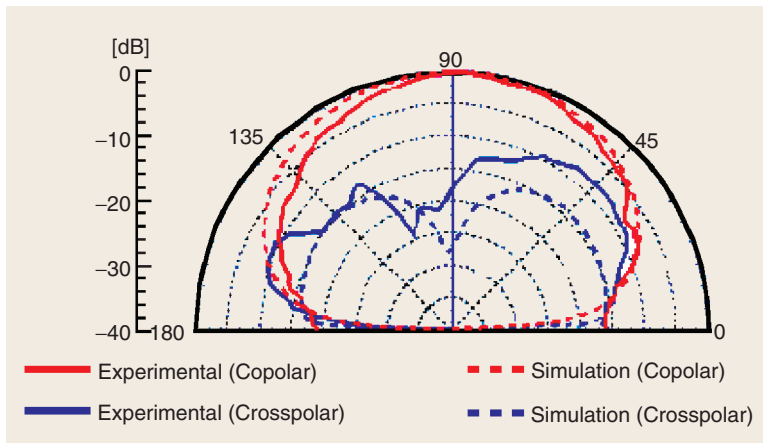
Figure 22. *Radiation patterns of the four-cell ZOR antenna [26].*

line. The width of each digit and of the meander line is 100 μm. The virtual ground patch size is 2.0×4.8 mm^2, and the antenna is matched to 50 Ω.

The measured and simulated (MoM) radiation patterns of the ZOR antenna are shown in Figure 22. The experimental results agree well with the simulated results. In addition, a -11 dB return loss was obtained.

Backfire-to-Endfire Leaky-Wave Antenna

The balanced CRLH TL of Figure 9(a) can be used as an efficient, frequency-scanned leaky-wave (LW) antenna when optimally matched to the air impedance [27]. A CRLH LW antenna has two distinct advantages over conventional LW antennas. First, a CRLH LW antenna can operate at its fundamental mode, because this mode contains a radiation (or fast-wave) region ($|\beta| < k_0$, where k_0 is the free-space propagation constant) in addition to a guided (or slow-wave) region ($|\beta| > k_0$), as shown in Figure 23(a). In contrast, RH structures have to be operated at higher order modes in order to radiate and, consequently, require a more complex and less-efficient feeding structure, because the

fundamental mode of RH structures are always guided ($\beta > k_0$). Second, a CRLH LW antenna is capable of continuous scanning from backward (backfire) to forward (endfire) angles, unlike conventional LW antennas. This can be seen by examining the LW antenna scanning angle equation

$$\theta = \sin^{-1}\left(\frac{\beta_0 + 2n\pi/p}{k_0}\right), \qquad (18)$$

where β_0 is the propagation constant of the fundamental mode, n is the space harmonic [28], and p is the period. For a nonperiodic LW antenna, $n = 0$, and β_0 is the propagation constant of the operating mode. For the CRLH LW antenna ($n = 0$, fundamental mode), θ can take on values from $-90°$ (backfire) to $+90°$ (endfire), since $|\beta| < k_0$ for a continuous frequency range as seen in Figure 23(a). Figure 23(b) depicts the scanning operation of the CRLH LW antenna. By operating the CRLH LW antenna below or above its transition frequency ω_0, forward and backward scanning is achieved. Referring to Figure 23, the antenna radiates backward in Region II (LH), and the antenna radiates forward in Region III (RH). At ω_0, the antenna is able to radiate broadside because $v_g \neq 0$ at $\beta = 0$ for the balanced CRLH TL. In contrast, a conventional nonperiodic LW antenna can only scan from broadside to endfire, since β is always positive. In addition, a conventional nonperiodic LW antenna cannot radiate at broadside because $v_g = 0$ (standing wave) at $\beta = 0$ for a RH structure. A conventional periodic LW antenna is able to scan from backfire to endfire by operating at negative and positive space harmonics ($n = \pm 1, \pm 2, \ldots$) [27], but broadside radiation cannot occur.
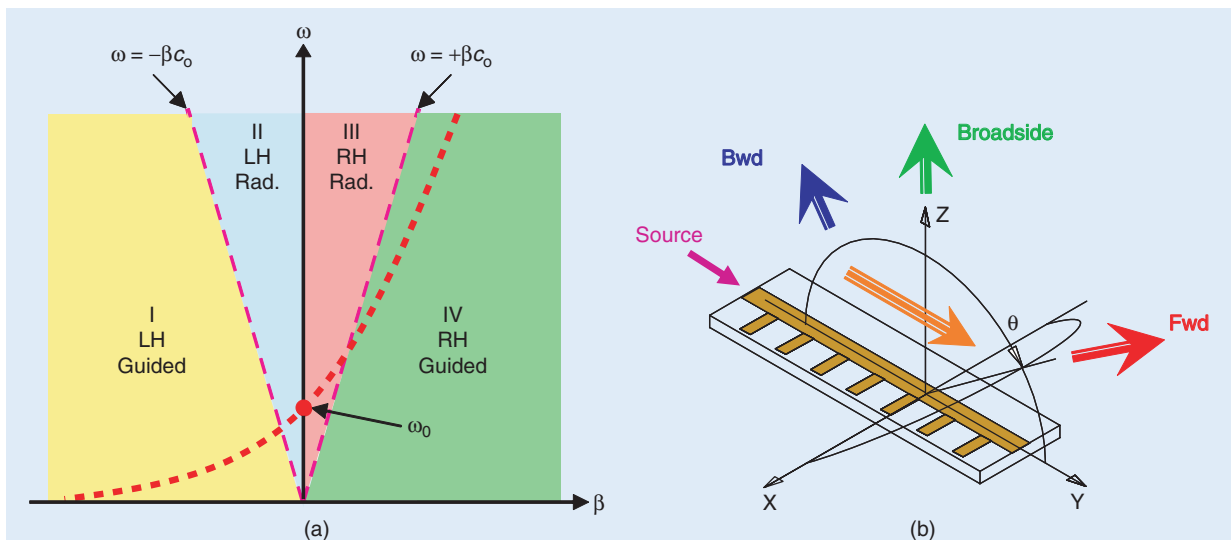

Figure 23. *CRLH LW Antenna. (a) Typical dispersion diagram showing guided and radiation regions. (b) Scanning operation.*
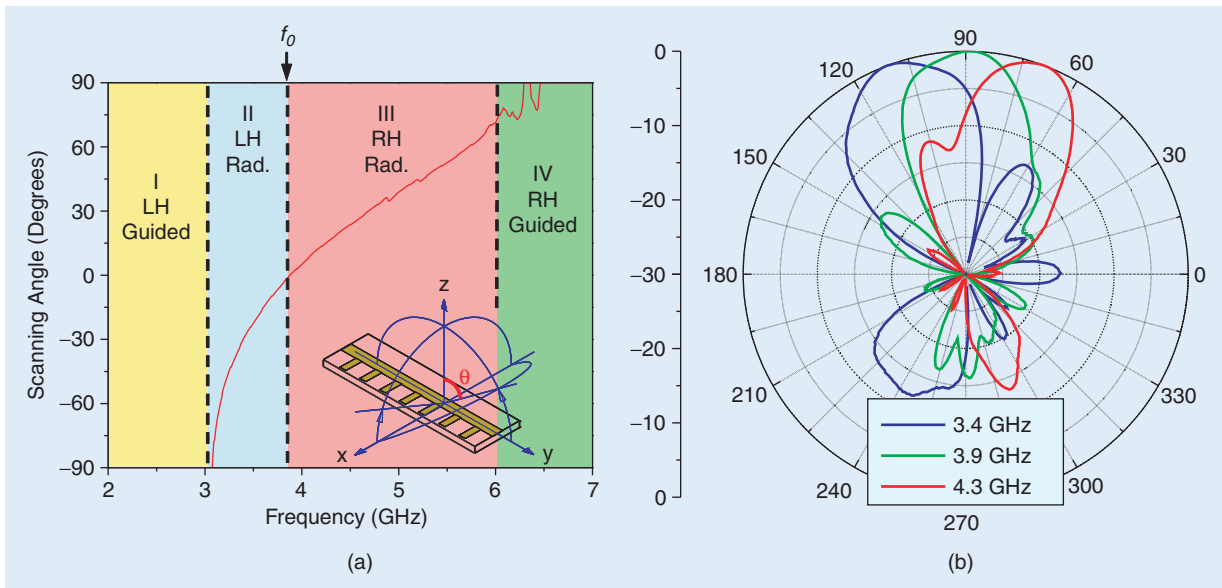
Figure 24. *Measured Results. (a) Scanning angle versus frequency [27]. (b) Radiation patterns for 3.4, 3.9, and 4.3 GHz [27].*

To radiate efficiently, the TL of Figure 9(a) is terminated with a matched load to eliminate reflections which would otherwise produce spurious beams. Continuous backfire-to-endfire scanning was achieved from 3.1 to 6.0 GHz, as displayed in Figure 24(a). Measured radiation patterns demonstrating backward, broadside, and forward scanning are shown in Figure 24(b).

Electronically Controlled LW Antenna

Like in most LW antennas, the scanning angle of the CRLH LW antenna discussed above is determined by its operation frequency. However, frequency-dependent LW antennas are not practical for most modern wireless communication systems, which generally operate at a fixed frequency for effective channelizing [29]. There have been several efforts to develop frequency-independent LW antennas [30]–[32]. However, most of the resulting antennas were only able to scan at two discrete angles or required a dc magnetic field supply, which is generally not practical for microwave applications. In [29], a frequency-independent LW antenna capable of continuous scanning and beamwidth control was realized with a TL composed of voltage-controlled CRLH unit cells. By controlling the bias voltage of varactor diodes included in the CRLH unit cell, the capacitance of the cell is changed. As a result, the propagation constant of the CRLH unit cell becomes a function of voltage as illustrated in Figure 25.

Since the voltage applied to each cell can be different, the voltage distribution on the antenna can be uniform or nonuniform. Depending on the type of voltage distribution, the antenna can be used as a scanning or beamwidth-controlling LW antenna. In the case of uniform distribution, the propagation constant of each unit cell is identical, and each cell radiates toward the same angle, so that directivity is maximal. Since β is a function of V, the scanning angle of (18) becomes

$$\theta(V) = \sin^{-1}\left(\frac{\beta(V)}{k_0}\right) \qquad (19)$$

for a fundamental mode ($n = 0$) LW antenna. Therefore, the antenna functions as a voltage-controlled scanning LW antenna when voltage is uniformly distributed. In contrast, under nonuniform voltage distribution, the propagation constant of each unit cell can be individually controlled, and each cell radiates towards a different angle, which results in a broader radiation beam. By controlling the voltage applied to each cell, the beam pattern of the antenna can be varied. Therefore, the antenna functions as a beamwidth-controllable LW
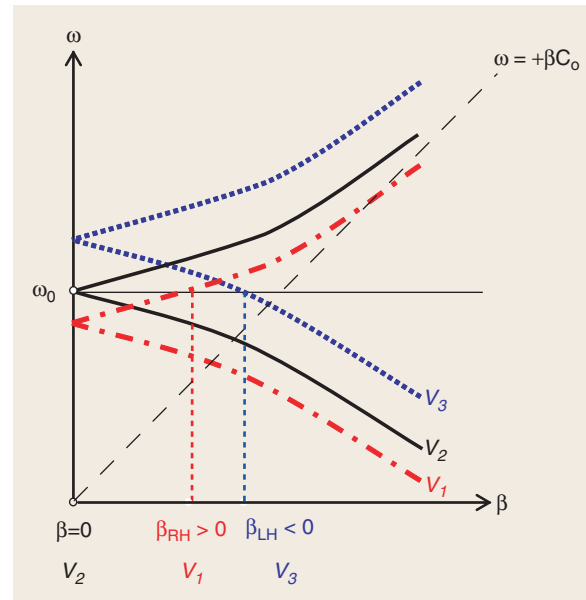

Figure 25. *Principle of voltage controlled CRLH unit cell. Dispersion curves are shifted vertically as the voltage is varied [29].*
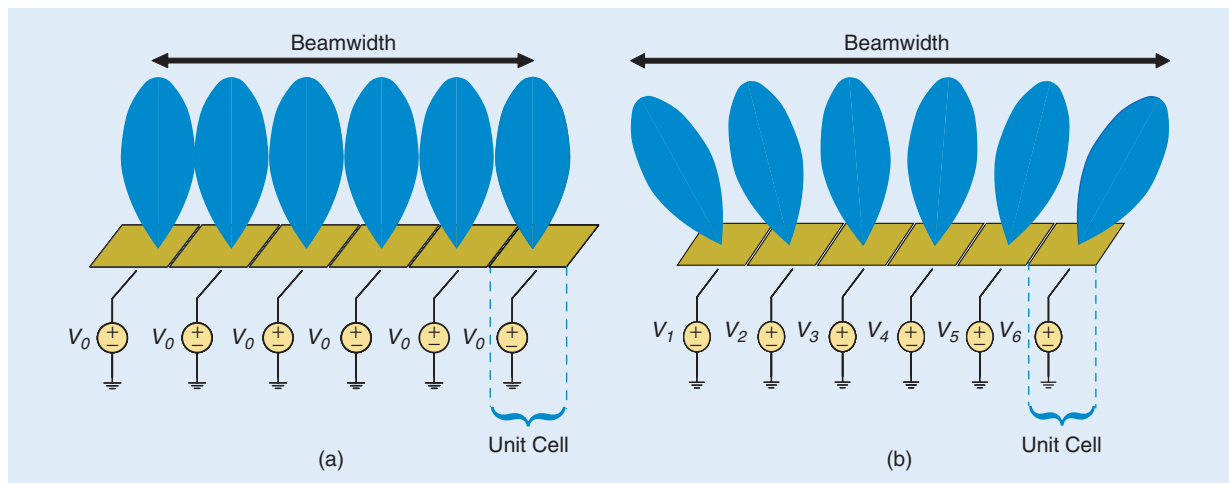
Figure 26. *Principle of beamwidth control. (a) Narrow beamwidth with uniform voltage distribution [29]. (b) Wide beamwidth with nonuniform voltage distribution [29].*

antenna when the cells are nonuniformly biased. This beamwidth control principle is illustrated in Figure 26.

Figure 27 shows the 30-cell, voltage-controlled, 3.33-GHz CRLH LW antenna presented in [29]. As seen in the inset of Figure 27, each unit cell consists of three varactor diodes, two in series and one in shunt configuration. This configuration was used to maintain constant characteristic impedance and attain high design flexibility [29]. The antenna was implemented on Rogers RT/Duroid 5880 with dielectric constant $\varepsilon_r = 2.2$ and thickness $h = 1.57$ mm. Metalics MSV 34060-E28X Si abrupt varactor diodes were used in the unit cells. Port 2 of the structure was terminated with a 50-Ω load to suppress spurious beams.

Figure 28 shows the theoretical and experimental scanning angle versus the reverse bias voltage relationship of the antenna under uniform biasing. By increasing the voltage, the antenna scans from backward to forward angles (99° range). A maximum gain of 18 dBi is observed at broadside. In [29], the half power beamwidth (HPBW) of the antenna under nonuniform biasing was also measured. The HPBW was increased by 43% to 200% compared to the uniformed biased case.
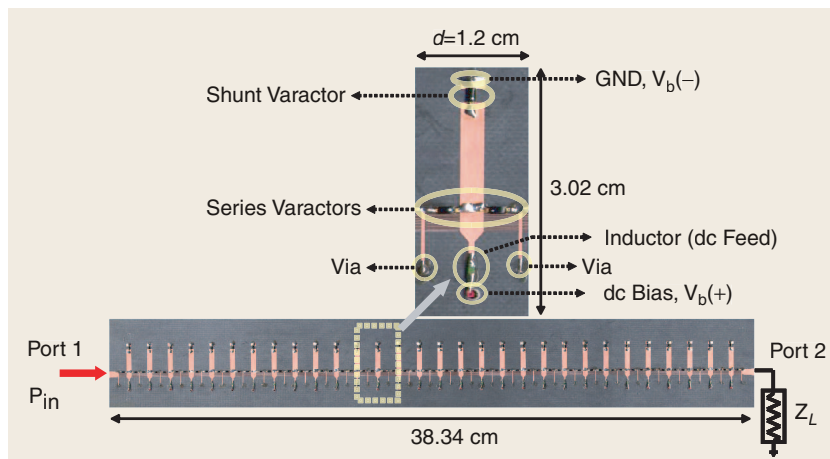
Other Radiated-Wave Applications

A novel reflectodirective system was demonstrated in [33] by combining a frequency-scanned CRLH LW antenna and heterodyne mixing. This system is able to receive an incident signal at any angle and reflect it at any arbitrary angle by tuning the local oscillator frequency. Fixed-frequency scanning can be achieved by using the electronically controlled CRLH LW antenna in place of the frequency-scanned CRLH LW antenna. The CRLH LW antennas discussed so far were only able to scan in one-dimension. By using an open mushroom structure similar to Figure 11(a) [34] demonstrated an LW antenna capable of 2-D scanning, which is useful for anticollision systems where full-space scanning is required. This 2-D CRLH LW antenna achieved a scanning range of 15–33° in the backward region and a 27–63° range in the forward region.

Refracted Wave Applications

Planar Negative Refractive Index Lens

In [14], a negative refractive index (NRI) planar lens was fabricated with the open mushroom structure of Figure 11(a) to demonstrate the reversal of Snell's Law. The NRI lens, consisting of a 20×6 CRLH unit cell array, was sandwiched between two RH parallel plate waveguides (PPWs). The completed NRI lens is shown in Figure 29(a), and a cross-sectional view is shown in Figure 29(b). The top view of the CRLH structure is shown in Figure 13(a), and the dispersion diagram of the mushroom unit cell used for the NRI lens is shown in Figure 12. A coaxial line source is placed 15 mm away

Figure 27. *A 30-cell electronically scanned LW antenna [29].*

from the CRLH structure to excite one of the PPWs. A focus will appear in the center of the CRLH structure if its refractive index (n_{LH}) is the negative of the refractive index (n_{PPW}) of the PPW ($n_{LH} = -n_{PPW}$).

At an operation frequency of 3.737 GHz, the CRLH structure possess a refractive index of $n_{LH} = -3.40$. In contrast, the PPW has a refractive index of $n_{PPW} = 2.77$. The coaxial source was excited at 3.737 GHz, and the field distribution above the LH structure was measured with a vertical probe on an automated stage. The magnitude and phase of the measured electric field are respectively shown in Figure 30(a) and (b). Despite the slight mismatch of the refractive indices, a focus can be observed in the LH structure. In [35], an NRI lens composed of SMT chip components produced similar results that demonstrated the reversal of Snell's Law.

Other Refracted Wave Applications

Although refractive, 2-D CRLH metamaterials are still at the level of conceptual demonstration, they are promising for imaging and polarization applications not possible with conventional RH materials. For example, an NRI lens with $\varepsilon = -1$ and $\mu = -1$, can achieve subwav-length focusing, as predicted by Pendry [36]. Such a lens will allow focusing of light in an area smaller than λ^2 and was verified by numerical simulations in [37]. In addition, anisotropic CRLH metamaterials, which exhibit a positive refractive index (PRI) in one direction and an NRI in an orthogonal direction, can be used to design polarization selective antennas/reflectors [38].

Conclusion

In this article, the fundamental properties of LHMs were discussed. In particular, an overview of the more general CRLH materials was presented based on an extended TL theory. Both 1- and 2-D CRLH TL structures were described, and various physical realizations of these structures were discussed. To demonstrate the practicality of CRLH TL structures, various guided, radiated, and refracted microwave applications were presented. These applications demonstrate that the TL approach of LHMs offers an efficient

alternative to the original physical realization of LHMs based on SRRs. This article has shown that low-loss, wide-bandwidth, and highly versatile LHMs are possible and constitute a very promising new paradigm for microwave and optical engineering.
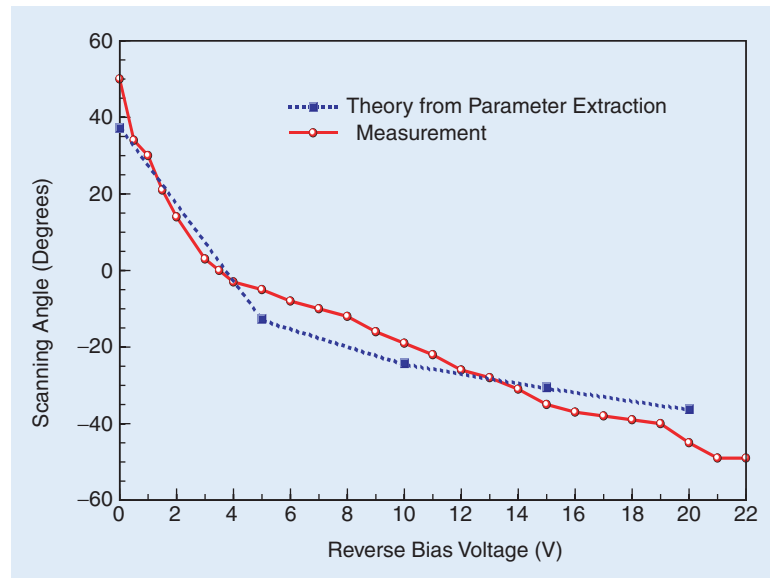

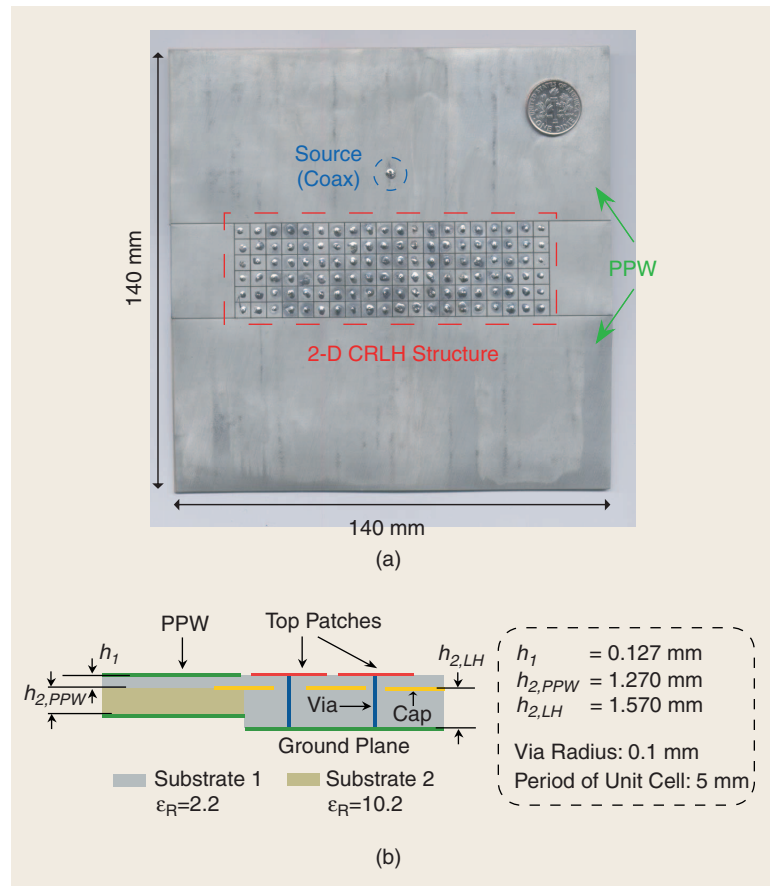**Figure 28.** *Measured and theoretical scanning angle versus reverse bias voltage [29].*

Figure 29. *NRI lens (20 × 6 cells). (a) Photograph of entire structure [14]. (b) Cross-sectional view.*
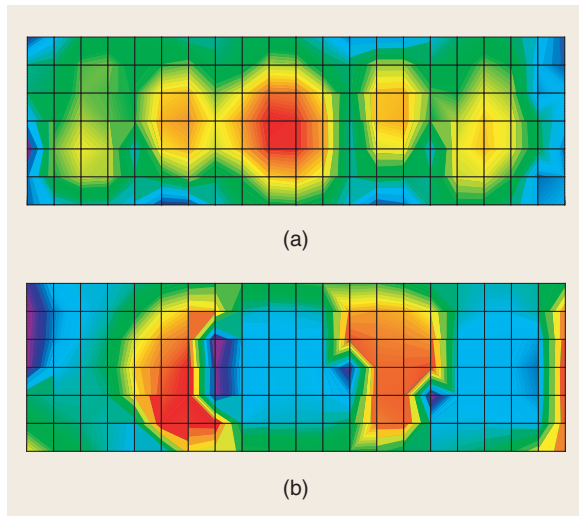
Figure 30. *Measured electric field distribution over the NRI lens of Figure 29. (a) Magnitude [14]. (b) Phase [14].*

References

[1] "Breakthrough of the year: The runners-up," *Science*, vol. 302, no. 5653, pp. 2039–2045, 2003.

[2] V. Veselago, "The electrodynamics of substances with simultaneously negative values of ε and μ," *Soviet Physics Uspekhi*, vol. 10, no. 4, pp. 509–514, 1968.

[3] S. Ramo, J.R. Whinnery, and T. Van Duzer, *Fields and Waves in Communication Electronics,* 2nd ed. New York: Wiley, 1984.

[4] R.A. Shelby, D.R. Smith, and S. Schultz, "Experimental verification of a negative index of refraction," *Science*, vol. 292, no. 5514, pp. 77–79, 2001.

[5] A.A. Houck, J.B. Brock, and I.L. Chuang, "Experimental observations of a left-handed material that obeys Snell's Law," *Phys. Rev. Lett.*, vol. 90, pp. 137–401, Apr. 2003.

[6] C.R. Simovski, P.A. Belov, and H. Sailing, "Backward wave region and negative material parameters of a structure formed by lattices of wires and split-ring resonators," *IEEE Trans. Antennas Propagat.*, vol. 51, pp. 2582–2591, Oct. 2003.

[7] E. Ozbay, K. Aydin, E. Cubukcu, and M. Bayindir, "Transmission and reflection properties of composite double negative metamaterials in free space," *IEEE Trans. Antennas Propagat.*, vol. 51, pp. 2592–2595, Oct. 2003.

[8] R.W. Ziolkowski and A.D. Kipple, "Application of double negative materials to increase the power radiated by electrically small antennas," *IEEE Trans. Antennas Propagat.*, vol. 51, pp. 2626–2640, Oct. 2003.

[9] C. Caloz, H. Okabe, T. Iwai, and T. Itoh, "Transmission line approach of left-handed (LH) materials," in *Proc. USNC/URSI National Radio Science Meeting*, San Antonio, TX, June 2002, vol. 1, p. 39.

[10] G.V. Eleftheriades, O. Siddiqui, and A.K. Iyer, "Transmission line models for negative refractive index media and associated implementations without excess resonators," *IEEE Microwave Wireless Compon. Lett.*, vol. 13, pp. 51–53, Feb. 2003.

[11] C. Caloz and T. Itoh, *Electromagnetic Metamaterials: Transmission Line Theory and Microwave Applications*. New York: Wiley, 2004.

[12] G.V. Eleftheriades, A.K. Iyer, and P.C. Kremer, "Planar negative refractive index media using periodically L-C loaded transmission lines," *IEEE Trans. Microwave Theory Tech.*, vol. 50, pp. 2702–2712, Dec. 2002.

[13] C. Kittel, *Introduction to Solid State Physics*, 7th ed. New York: Wiley, 1964.

[14] A. Sanada, C. Caloz, and T. Itoh, "Planar distributed structures with negative refractive properties," *IEEE Trans. Microwave Theory Tech.*, vol. 52, pp. 1252–1263, Apr. 2004.

[15] D. Sievenpiper, L. Zhang, F.J. Broas, N.G. Alexopulos, and E. Yablonovitch, "High-impedance electromagnetic surfaces with a forbidden frequency band," *IEEE Trans. Microwave Theory Tech.*, vol. 47, pp. 2059–2074, Nov. 1999.

[16] R.E. Collin, *Field Theory of Guided Waves*, 2nd ed. New York: Wiley-Interscience, 1991.

[17] I. Lin, C. Caloz, and T. Itoh, "A branch-line coupler with two arbitrary operating frequencies using left-handed transmission lines," in *IEEE-MTT Int. Symp. Dig.*, Philadelphia, PA, 2003, vol. 1, pp. 325–327.

[18] I. Lin, M. DeVincentis, C. Caloz, and T. Itoh, "Arbitrary dual-band components using composite right/left-handed transmission lines," *IEEE Trans. Microwave Theory Tech.*, vol. 52, pp. 1142–1149, Apr. 2004.

[19] C. Caloz and T. Itoh, "A novel mixed conventional microstrip and composite right/left-handed backward-wave directional coupler with broadband and tight coupling characteristics," *IEEE Microwave Wireless Compon. Lett.*, vol. 14, pp. 31–33, Jan. 2004.

[20] R. Mongia, I. Bahl, and P. Bhartia, *RF and Microwave Coupled-Line Circuits*. Norwood, MA: Artech, 1999.

[21] C. Caloz, A. Sanada, and T. Itoh, "A novel composite right/left-handed coupled-line directional coupler with arbitrary coupling level and broad bandwidth," *IEEE Trans. Microwave Theory Tech.*, vol. 52, pp. 980–992, Mar. 2004.

[22] A. Sanada, C. Caloz, and T. Itoh, "Zeroth order resonance in composite right/left-handed transmission line resonators," in *Proc. Asia-Pacific Microwave Conf.*, Seoul, Korea, 2003, vol. 3, pp. 1588–1592.

[23] H. Okabe, C. Caloz, and T. Itoh, "A compact enhanced-bandwidth hybrid ring using an artificial lumped-element left-handed transmission-line section," *IEEE Trans. Microwave Theory Tech.*, vol. 52, pp. 1142–1149, Apr. 2004.

[24] C. Caloz, I. Lin, and T. Itoh, "Characteristics and potential applications of nonlinear left-handed transmission lines," *Microwave and Optical Tech. Lett.*, vol. 40, no. 6, pp. 471–473, Mar. 2004.

[25] T. Fujishige, C. Caloz, and T. Itoh, "Experimental demonstration of the ENG-MNG pair resonator in a CRLH transmission line implementation," *IEEE Trans. Microwave Theory Tech., submitted.*

[26] A. Sanada, M. Kimura, I. Awai, H. Kubo, C. Caloz, and T. Itoh, "A planar zeroth order resonator antenna using left-handed transmission line," to be presented at the European Microwave Conf., Amsterdam, Netherlands, 2004.

[27] L. Liu, C. Caloz, and T. Itoh, "Dominant mode (DM) leaky-wave antenna with backfire-to-endfire scanning capability," *Electron. Lett.*, vol. 38, no. 23, pp. 1414–1416, 2000.

[28] S. Majumder, D.R. Jackson, A.A. Oliner, and M. Guglielmi, "The nature of the spectral gap for leaky waves on a periodic strip-grating structure," *IEEE Trans. Microwave Theory Tech.*, vol. 45, pp. 2296–2307, Dec. 1997.

[29] S. Lim, C. Caloz, and T. Itoh, "Metamaterial-based electronically controlled transmission line structure as a novel leaky-wave antenna with tunable radiation angle and beamwidth," *IEEE Trans. Microwave Theory Tech., submitted.*

[30] R.E. Horn, H. Jacobs, E. Freibergs, and K.L. Klohn, "Electronic modulated beam steerable silicon waveguide array antenna," *IEEE Trans. Microwave Theory Tech.*, vol. 28, pp. 647–653, June 1980.

[31] H. Maheri, M. Tsutsumi, and N. Kumagi, "Experimental studies of magnetically scannable leaky-wave antennas having a corrugated ferrite slab/dielectric layer structure," *IEEE Trans. Antennas Propagat.*, vol. 36, pp. 911–917, July 1988.

[32] L. Huang, J. Chiao, and M.P. DeLisio, "An electronically switchable leaky wave antenna," *IEEE Trans. Antennas Propagat.*, vol. 48, pp. 1769–1772, Nov. 2000.

[33] S. Lim, C. Caloz, and T. Itoh, "A reflecto-directive system using a composite right/left-handed (CRLH) leaky-wave antenna and heterodyne mixing," *IEEE Microwave Wireless Compon. Lett.*, vol. 14, pp. 183–185, Apr. 2004.

[34] C. Allen, C. Caloz, and T. Itoh, "Leaky-waves in a metamaterial-based two-dimensional structure for a conical beam antenna application," presented at the IEEE-MTT Int. Symp., Fort Worth, TX, 2004.

[35] A.K. Iyer, P.C. Kremer, and G.V. Eleftheriades, "Experimental and theoretical verification of focusing in large, periodically loaded transmission line negative refractive index metamaterial," *Optics Express*, vol. 11, no. 7, pp. 696–708, Apr. 2003.

[36] J.B. Pendry, "Negative refraction makes a perfect lens," *Phys. Rev. Lett.*, vol. 85, pp. 3966–3969, Oct. 2000.

[37] A. Grbic and G.V. Eleftheriades, "Subwavelength focusing using a negative-refractive-index transmission line lens," *IEEE Antennas Wireless Propagat. Lett.*, vol. 2, no. 13, pp. 186–189, 2003.

[38] C. Caloz and T. Itoh, "Positive/negative refractive index anisotropic 2-D metamaterials," *IEEE Microwave Wireless Compon. Lett.*, vol. 13, pp. 547–549, Dec. 2003.